DOI:
10.1115/1.4039002

Document Version
Peer reviewed version

Branch reconfiguration of Bricard linkages based on toroids intersections: Plane-symmetric case.

P. C. López-Custodio*

Centre for Robotics Research,
King's College London,
University of London,
Strand, London WC2R 2LS, UK
Email: pablo.lopez-custodio@kcl.ac.uk

J.S. Dai

Centre for Robotics Research,
King's College London,
University of London,
Strand, London WC2R 2LS, UK
Email: jian.dai@kcl.ac.uk

J. M. Rico

Mechanical Engineering Department,
DICIS, Universidad de Guanajuato,
Salamanca, Guanajuato, Mexico
Email: jrico@ugto.mx

This paper for the first time investigates a family of plane-symmetric Bricard linkages studying two generated toroids. By means of their intersection, a set of special Bricard linkages with various branches of reconfiguration are designed. An analysis of the intersection of these two toroids reveals the presence of coincident conical singularities which lead to the design of plane-symmetric linkages that evolve to spherical 4R linkages. By examining the tangents to the curves of intersection at the conical singularities it is found that the linkage can be reconfigured between the two possible branches of spherical 4R motion without disassembling it and without requiring the usual special configuration connecting the branches.

The study of tangent intersections between concentric singular toroids also reveals the presence of isolated points in the intersection which suggests that some linkages satisfying the Bricard plane-symmetry conditions are actually structures with zero finite degrees of freedom but with higher instantaneous mobility. This paper is the second part of a paper submitted in parallel by the authors in which the method is applied to the line-symmetric case.

1 Introduction

Among the reported overconstrained linkages, the Bricard linkages (along with the famous Bennett 4R linkage) are the most studied due to their very special geometry that allow the mobility of these 6R loops. A total of six cases were discovered by Bricard [1, 2]: the line-symmetric case, the plane-symmetric case, the trihedral case, the line-symmetric octahedral case, the plane-symmetric octahedral case and the doubly collapsible octahedral case. The geometry of these loops was thoroughly studied [3] [4] [5] [2] in order to explain the mobility of these linkages. However, some other properties of the Bricard linkages are still being studied, including optimization, application, combination of loops in large structures and reconfigurability, which has not been systematically analized and whose intuitive presence on the linkages has not been revealed. This paper deals with these issues.

A reconfigurable linkage [6] has a configuration space that includes at least two space components that are connected through singular configurations. Thus, the linkage can work in different motion branches without being disassembled [7]. If these connected components of the configuration space are of different dimensions, then the linkage is able to change its degrees of freedom or local mobility and it is said to be a *kinematotropic* linkage [8, 9]. At the constraint singularity with change of joint functionality or link annexation resulting in configuration space change, a different kind of reconfigurable linkage emerges as the *metamorphic* linkages [10, 11, 12, 13]. Recent advances in reconfigurable linkages include: a closed chain with 14 states that constitute 28 configurations [14], a reconfigurable platform whose hybrid legs include a 4R diamond [15], a parallel manipulator with 15 motion branch [16], type synthesis of kinematotropic platforms [17], various reconfigurable kinematic

*Address all correspondence to this author.

chains with mobility one [18], a family of single-loop reconfigurable linkages with an infinity of motion branches [19]. Some advances in the study of reconfigurable linkages include: the analysis of the connections between components of the configuration space by means of algebraic geometry [20], the study of reconfigurability by means of reciprocity of screws [21], the use of morphing systemization to analyze ways of reconfiguration of linkages [22], the application of higher order kinematic analysis to prove the local mobility of kinematotropic linkages [23,24,25] and the application of dual quaternions in the analysis of reconfigurability [26,16].

In regard to Bricard linkages that lead to different motion branches, the following contributions have already been presented: the analysis of reconfiguration of a plane- and line-symmetric Bricard linkage by means of geometric constraints and screw-system variations [18], spatial triangle formed joint and variable axis joint are used to obtain a line-symmetric linkage that can behave as a Bennett linkage [27], the analysis of a plane- and line-symmetric Bricard linkage with different motion branches in order to avoid singularities [28] and a line-symmetric Bricard linkage evolved from a metamorphic 8R linkage [29]. In these studies, a theory of the reconfigurability of Bricard loops that can help the design of these linkages has not been studied thoroughly. However, the authors searched for a method that could be used for this study and the method of generated surfaces appeared as a very promising alternative.

The technique of generated surfaces, based on kinematic dyads joined by spherical pairs or any possible reduction [30, 31, 32], was formerly applied to prove the mobility of some overconstrained linkages [33], design of linkages with dwell motion [34], analysis of non-overconstrained linkages [35], synthesis of parallel platforms [36] and software graphics [37]. The method was recently applied to reconfigurable linkages [38, 19, 39], taking advantage of the rich knowledge on tangent intersection of surfaces.

In this paper, the method is for the first time applied to the branch reconfiguration of Bricard plane-symmetric linkages, following the previous paper in which the authors study the line-symmetric case. The plane-symmetric case is characterized by the following DH parameters [5]:

$$\begin{aligned} &a_{6,1} = a_{1,2}, a_{2,3} = a_{5,6}, a_{3,4} = a_{4,5}, \\ &\alpha_{1,2} + \alpha_{6,1} = 2\pi, \alpha_{2,3} + \alpha_{5,6} = 2\pi, \alpha_{3,4} + \alpha_{4,5} = 2\pi, \\ &d_1 = d_4 = 0, d_2 = -d_6, d_3 = -d_5. \end{aligned} \quad (1)$$

where the positive direction of the z_i axes[1] is given by the screw direction shown in Fig. 1. In this case each member of the linkage is symmetric to another member through a plane π (Fig. 1). Therefore, axes S_2 and S_6 (S_3 and S_5) intersect in a point lying on π and axes S_1 and S_4 also lie on π. Hence, a line containing the points of intersection of pairs of axes $\{S_2, S_6\}$ and $\{S_5, S_3\}$ lies on π and, therefore also intersects S_1 and S_4. Such line is the central axis of the linear complex [40,41,3,42] which the six axes belong to. The pitch of such linear complex is zero since the central axis always intersects the six axes.

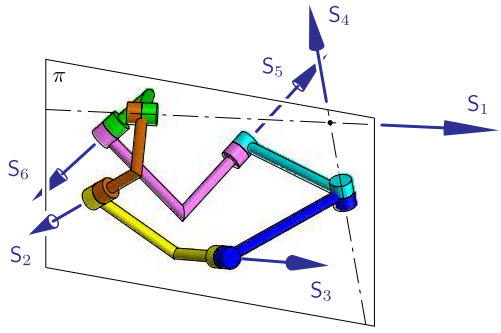

Fig. 1. The general plane-symmetric case of Bricard linkage.

The plane-symmetric Bricard linkage is analyzed in this paper by means of the intersection of two generated toroids, building a complete theory of the reconfigurability of these loops. The design is made by manipulating the construction parameters of two concentric singular toroids. An interesting result is the discovery of spherical 4R linkages evolved from the plane-symmetric linkages that are always able to reconfigure between their two branches without being disassembled and without passing through the special configuration that connects the branches in common 4R linkages. To the knowledge of the authors, this is the first time that a linkage with such reconfiguration between disjoint spherical 4R branches is presented and studied. However, Bricard 6R linkages that also work as spherical 4R linkages were first presented in [43].

This paper is organized as follows: The toroids, its generators and its singular forms are revisited in Section 2. Then, in Section 3, it is find out that some examples of Bricard plane-symmetric linkages can be explained and designed as the intersection of concentric singular toroids. This intersection is analyzed in Section 4. In Section 5 any possibility of tangent intersection is explored. In Section 5 the two branches of spherical 4R motion are studied in order to figure out how to reconfigure the linkage from Bricard branches to spherical 4R branches. Finally, two examples are presented in Section 7. This paper is a continuation of the paper submitted by the authors on the line-symmetric case, [44], some theory, notation, and basic concepts used here are introduced in the aforementioned.

2 Singular toroids generated by kinematic RR chains.

In the second section in the paper submitted by the authors on the line-symmetric case, [44], a discussion on general toroids generated by RR dyads was presented. Now, the particular case in which the radius of the secondary and base circles are the same, $l = r$, and there is no secondary offset,

[1] In [5] Baker sets the positive direction in such a way that the parameters d_i are always positive, obtaining DH parameters slightly different but equivalent to the ones used in this paper, where the directions are simply reflected by plane π in figure 1.

$s=0$, is discussed. Such a toroid, $T_{r,r,\gamma,0}$, can be generated by the following parameterization:

$$\sigma(u,v) = r\Big((\cos v+1)\cos u - \cos\gamma\sin v\sin u,\\ \cos\gamma\sin v\cos u + (\cos v+1)\sin u,\ \sin\gamma\sin v\Big) \in \mathbb{R}^3 \tag{2}$$

and $T_{l,r,\gamma,s} = \mathrm{im}(\sigma(\mathbb{T}^2))$. In a similar way, the implicit form $\phi \in \mathbb{R}[x,y,z]$ is reduced to:

$$\phi(x,y,z) = \left(x^2+y^2+z^2-2r^2\right)^2 - 4r^2\left(r^2 - \frac{z^2}{\sin^4\gamma}\right) \tag{3}$$

and $T_{r,r,\gamma,s} = \left\{\mathbf{r}_E \in \mathbb{R}^3 \,|\, \phi(\mathbf{r}_E)=0\right\}$. For this case, it is easy to prove that:

$$\left.\frac{\partial\sigma}{\partial u}\right|_{(u,v)=(u,\pi)} = \mathbf{0} \Rightarrow \left.\left(\frac{\partial\sigma}{\partial u}\times\frac{\partial\sigma}{\partial v}\right)\right|_{(u,v)=(u,\pi)} = \mathbf{0},\ \forall u\in\mathbb{T},$$

Therefore it can be concluded that $(u,\pi)\in\mathbb{T}^2$ is a conical singularity of $T_{r,r,\gamma,0}$. Hence, we call $T_{r,r,\gamma,0}$ a *singular toroid*[2]. In this case the singularity maps to the point $\sigma(u,\pi)=\mathbf{0}=O$. Figure 2 shows $T_{r,r,\gamma,0}$ with the singularity coincident with the origin. $\mathscr{B}$, the intersection of the toroid and any plane containing the Z axis, becomes an 8-shapped curve that is symmetric with respect to the intersection of the XY plane and the plane containing $\mathscr{B}$. The self-crossing of $\mathscr{B}$ occurs at O.

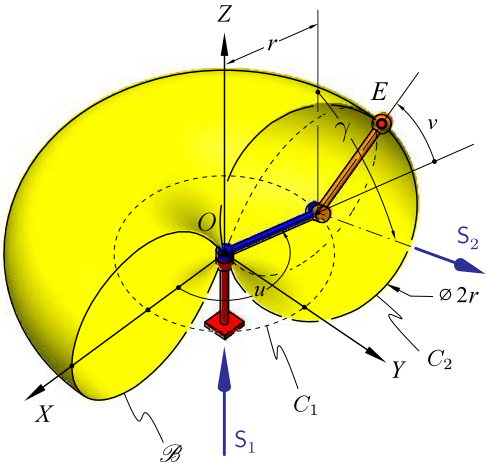

Fig. 2. An RR dyad generating a singular toroid ($r=l, s=0$).

[2]Conical singularities also appear when $\gamma=\pi/2$ and $r>l$. This is a singular right torus, two conical singularities appear symmetrically disposed in the Z axis. This class of torus never appear in plane-symmetric linkages and thus they are not considered in this paper.

3 The concentric singular toroids generated by the plane-symmetric Bricard linkage.

In the plane-symmetric case of Bricard linkage any adjacent pair of revolute joints with skew axes generates a toroid. For a general plane-symmetric linkage, like the one shown in Fig. 1, let $a_{2,3}=0$. Then the point of intersection of S_2 and S_3 describes a toroid with respect to the fixed link between axes S_6 and S_5, this is generated by joints with axes S_6 and S_1. Furthermore, the same point describes another toroid with respect to the fixed link, this time generated by joints with axes S_4 and S_5. Since the same point describes two toroids, such point is confined to move in the intersection of these toroids.

From the restrictions for plane symmetry in Eq. (1) , observe that if $a_{2,3}=0$ then $a_{5,6}=0$. This implies that both toroids are concentric, as shown in Fig. 3a. Furthermore, since $a_{6,1}=a_{1,2}$ and $a_{3,4}=a_{4,5}$, then $r=l$ for both toroids. Finally, since $d_1=d_4=0$ both toroids have secondary offset $s=0$. From these observations it can be concluded that both generated toroids are singular, with the singularity coinciding with the intersection of fixed axes S_6 and S_5. Summarizing, in addition to the restrictions on the DH parameters of the plane-symmetric linkage in Eq. (1), the following conditions are required to analyze and design these linkages using the intersection of two toroids:

$$\begin{aligned} &\bullet\ d_i=0,\ i=1,\dots,6\\ &\bullet\ a_{2,3}=a_{5,6}=0 \end{aligned} \tag{4}$$

Fig. 3b shows an example of plane-symmetric Bricard linkage that generates two singular toroids. For the sake of identifying the construction parameters of each toroid, the joints have been renamed with respect to Fig. 1: $\mathsf{S}_{A1}=\mathsf{S}_6$, $\mathsf{S}_{A2}=\mathsf{S}_1$, $\mathsf{S}_{A3}=\mathsf{S}_2$, $\mathsf{S}_{B3}=\mathsf{S}_3$, $\mathsf{S}_{B2}=\mathsf{S}_4$ and $\mathsf{S}_{B1}=\mathsf{S}_5$. In such case, a singular toroid $T^i_{r_i,r_i,\gamma_i,0} := T_{r_i,r_i,\gamma_i,0}(\hat{\mathbf{k}}_i,O)$ is generated by the joints with axes S_{i1} and S_{i2} and is referred to coordinate systems i, $i=A,B$. The point that describes the intersection $\mathcal{C} := T^A_{r_A,r_A,\gamma_A,0} \cap T^B_{r_B,r_B,\gamma_B,0}$ is the intersection of axes S_{A3} and S_{B3} and is called E. The point where S_{A1} and S_{B1} intersect is called O.

For each toroid $T^i_{r_i,r_i,\gamma_i,0} := \{E_i(\mathbf{q}_i)\,|\,\mathbf{q}_i\in\mathbb{T}^2\}$, $i=A,B$, the joint variables vector is given by the variables of the parameterization in Eq. (2), so that $\mathbf{q}_i=(u_i,v_i)\in\mathbb{T}^2$. Once the link D joins axes S_{A3} and S_{B3}, $E_A(\mathbf{q}_A)=E_B(\mathbf{q}_B)=E(\mathbf{q})$, where $\mathbf{q} := (u_A, v_A, q_{A3}, q_{B3}, v_B, u_B) \in V \subset \mathbb{T}^6$, where V is the configuration space of the linkage whose elements have to fulfill the closure equation of the loop. Observe that, due to symmetry, q_{A3} and q_{B3} are in linear correspondence with u_A and u_B, respectively. Hence, finding the intersection $\mathcal{C}$ completely describes the behavior of the linkage. In fact, finding a parameterization of $\mathcal{C}$ in terms of any of the four variables of the toroids would be equivalent to solve the position analysis of the linkage.

$\mathcal{C}$ may be composed of several components such that $\mathcal{C}=\cup_{i=1}^n \mathcal{C}_i$, where $\dim(\mathcal{C}_i)\le 2$ and $n\in\mathbb{Z}^*$. Each component of $\mathcal{C}$ is related to a component of the configuration space V. When $\mathcal{C}_i$ is a curve $\mathscr{C}\subset\mathcal{C}$, $\dim(V_i)=1$, where V_i is

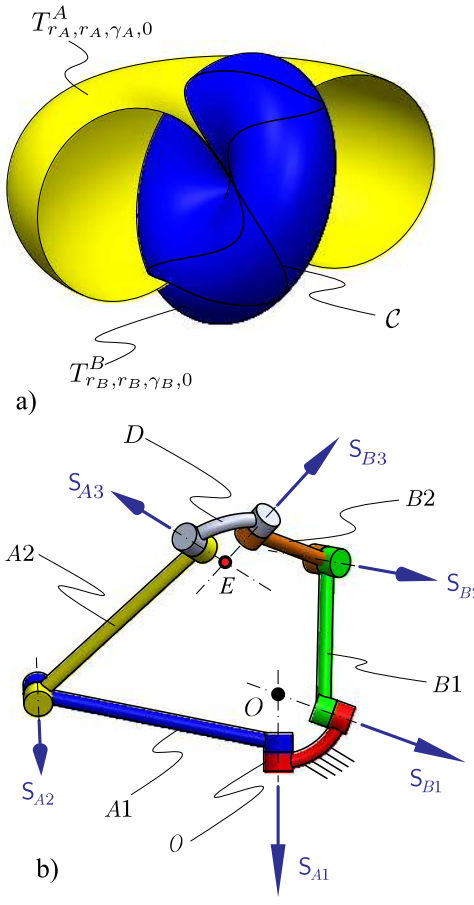

Fig. 3. The concentric singular toroids intersection: a) surfaces, b) resultant Bricard plane-symmetric linkage.

the corresponding component of V, and the linkage has 1 D.O.F. when assembled in this mode, this leads to the typical overconstrained behavior of the linkage. On the other hand, if C_i is an isolated point and $\dim(V_i) = 0$. In such component of V, the linkage can be assembled as a structure.

An important phenomenon occurs when two conical singularities coincide. We call this coincidence the *double singularity*. The arrangement of singular toroids for plane-symmetric linkages includes a double singularity since both toroids are concentric. In the general method of generated surfaces the two generators are connected by a spherical pair, it was proved [38] that for such linkages when E is in the double singularity the linkage has 2 D.O.F. since variables u_A and u_B can take any value without restriction while v_A and v_B remain constant. However, for the problem of plane-symmetric Bricard linkages the spherical pair has been reduced to a pair of coincident revolute joints. When E reaches the double singularity it coincides with O, therefore the axes S_{A1}, S_{B1}, S_{A3} and S_{B3} are intersecting in the double singularity while the joints with axes S_{A2} and S_{B2} remain idle. u_A and u_B are now dependent one from another since the linkage becomes a spherical 4R linkage. This property will be thoroughly studied in section 8.

Refer to figure 4 which shows the common perpendiculars diagram of the plane-symmetric linkage obtained from the intersection of two toroids. In any configuration the

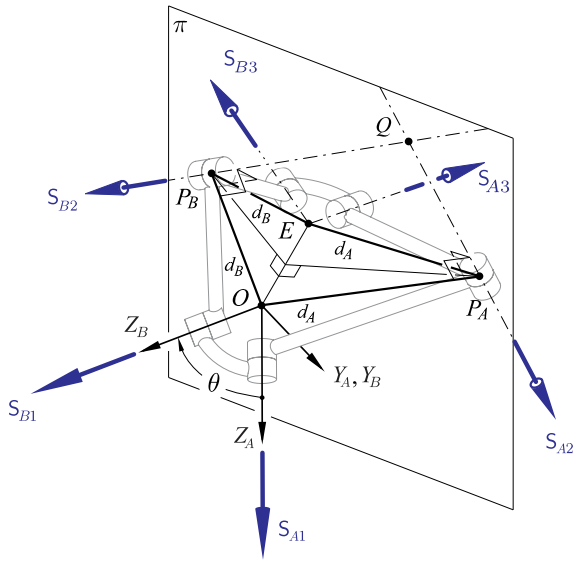

Fig. 4. Common perpendicular diagram for the plane-symmetric linkage.

common perpendiculars between the adjacent joint axes conform two isosceles triangles, OP_AE and OP_BE, these triangles share the same base OE, the lines from the mid-point of EO to P_A and P_B are perpendicular to OE and therefore, a plane π containing these two lines is perpendicular to the planes that contain the two triangles. The axes S_{A2} and S_{B2} contain P_B and P_A, respectively, and are perpendicular to the planes including the triangles OP_AE and OP_BE, respectively. Hence, both axes belong to π and therefore they either intersect or are parallel. This ensures that the symmetry condition is always present while E moves through all the components of $\mathcal{C}$.

4 Concentric singular toroid-toroid intersection.

To analyze the intersection of toroids in the plane-symmetric case, $\mathcal{C} = T^A_{r_A,r_A,\gamma_A,0} \cap T^B_{r_B,r_B,\gamma_B,0}$, let the relationship between coordinate systems A and B be given by ${}^A_B\mathbf{T} = \mathbf{T}(\mathbf{R}(\theta,\hat{\mathbf{j}}),\mathbf{0})$, so that the toroids are concentric and the axis of B is obtained by rotating the axis of A θ radians about the $Y := Y_A = Y_B$ axis.

The parameterizations of both surfaces referred to coordinate system A are:

$$
\begin{aligned}
{}^A\sigma_A(u_A,v_A) = \Big(& r_A\left((\cos v_A+1)\cos u_A - \cos\gamma_A \sin v_A \sin u_A\right), \\
& d_A\left(\cos\gamma_A \sin v_A \cos u_A + \sin u_A \cos v_A + \sin u_A\right), \\
& \sin\gamma_A d_A \sin v_A \Big)
\end{aligned}
$$

$$
\begin{aligned}
{}^A\sigma_B(u_B,v_B) = \Big(& (((\cos v_B+1)\cos u_B - \cos\gamma_B \sin v_B \sin u_B)\cos\theta \\
& + \sin\theta \sin\gamma_B \sin v_B) d_B,\ d_B(\cos\gamma_B \sin v_B \cos u_B + \\
& \sin u_B \cos v_B + \sin u_B),\ d_B(((-\cos v_B - 1)\cos u_B \\
& + \cos\gamma_B \sin v_B \sin u_B)\sin\theta + \cos\theta \sin\gamma_B \sin v_B) \Big)
\end{aligned}
\tag{5}
$$

and the implicit forms are given by:

$$
\begin{aligned}
{}^{A}\phi_A(x,y,z) &= \left(x^2+y^2+z^2-{r_A}^2-{r_B}^2\right)^2-4{r_B}^2\left({r_A}^2-\frac{z^2}{\sin^2\gamma_A}\right)\\
{}^{A}\phi_B(x,y,z) &= \frac{1}{\sin^2\gamma_B}\Big[-(x^2+y^2+z^2)(x^2+y^2+z^2-4{r_B}^2)\cos^2\gamma_B\\
&\quad+(-4x^2{r_B}^2+4z^2{r_B}^2)\cos^2\theta+8\cos\theta\sin\theta xz{r_B}^2+z^4\\
&\quad+(2x^2+2y^2-4{r_B}^2)z^2+x^4+2x^2y^2+y^4-4y^2{r_B}^2\Big]
\end{aligned}
\tag{6}
$$

A direct way to find $\mathcal{C}$ is to solve ${}^{A}\sigma_A - {}^{A}\sigma_B = \mathbf{f}(u_A,v_A,u_B,v_B) = \mathbf{0}$. However, in this case it turns out to be more complicated. An alternative technique, taken from [45], is applied instead: Since, for any of both implicit forms referred to coordinate system A, $(x,y,z) = {}^{A}\sigma_A(u_A,v_A) = {}^{A}\sigma_B(u_B,v_B)$, then ${}^{A}\phi_B({}^{A}\sigma_A(u_A,v_A)) = 0$ is a scalar equation with two variables from which the restrictions $u_A(v_A)$ or $v_A(u_A)$ can be obtained. This restriction fully defines $\mathcal{C}$ since it can be replaced in ${}^{A}\sigma_A$ to obtain the whole parameterization of the intersection, for example using the restriction $u_A(v_A)$: ${}^{A}\mathcal{C} = \{{}^{A}\sigma_A(u_A(v_A),v_A)\,|\,v_A \in W \subset \mathbb{T}\}$. Consider the parameterization of A being substituted in the implicit form of B:

$$
\begin{aligned}
&{}^{A}\phi_B({}^{A}\sigma_A(u_A,v_A)) = -\frac{4r_A^2}{\sin^2\gamma_B}(\cos v_A+1)\Big[r_B^2\cos^2\gamma_A(\cos v_A\\
&-1)(\sin^2 u_A+(\cos^2 u_A-2)\cos^2\theta)-r_B^2(\cos v_A+1)\cos^2 u_A\\
&-2r_B^2\sin u_A\cos\gamma_A(\sin\gamma_A\sin\theta\cos\theta(\cos v_A-1)\\
&-\cos u_A\sin v_A\sin^2\theta)+r_B^2\cos^2\theta((\cos v_A+1)\cos^2 u_A+\cos v_A-1)\\
&-2r_B^2\sin\gamma_A\cos\theta\sin\theta\sin v_A\cos u_A-\sin^2\gamma_B(\cos v_A+1)(r_A^2(1\\
&+\cos v_A)-2r_B^2)\Big]=0
\end{aligned}
\tag{7}
$$

An immediate first possibility is observed: $v_A = \pi$. This solution leads to the double singularity in which $E(\mathbf{q}) = O, \forall \mathbf{q} \in V_1$, where V_1 is the spherical $4R$ component of V related to the double singularity. Since making 0 the first factor in Equation 7 would compromise the construction parameters of the toroids, the only remaining possibility is solving the third factor. This factor is solved to obtain the restriction $u_A(v_A)$, two solutions are found which are not presented here due to reasons of space since these are quite long expressions. In a similar manner, two solutions for the restriction $v_A(u_A)$ are obtained. Therefore, $\mathcal{C}$ may feature a maximum of two curves. Expressions for a parameterization of these components can be computed as explained in the previous paragraph, however, due to the length of the terms involved in the restriction $u_A(v_A)$, these are not presented here.

5 Tangent intersections of concentric singular toroids.

If in the concentric toroid-toroid intersection $\exists i,j \ni \mathcal{C}_i \cap \mathcal{C}_j \neq \emptyset$ the linkage is reconfigurable with at least 2 motion branches, which are connected through at least one configuration $\mathbf{q}_{ij} \in V_i \cap V_j$. It can be proved [38] that for the 1-dimensional components of V, the toroids are tangent to each other at $E(\mathbf{q}_{ij})$. The intersection is non-transverse in $E(\mathbf{q}_{ij})$. Therefore, $\nabla\phi_A(x^P,y^P,z^P) \times \nabla\phi_B(x^P,y^P,z^P) = \mathbf{0}$, where $(x^P,y^P,z^P) = E(\mathbf{q}_{ij})$. The points in V that map to points of tangency *may* be bifurcation configurations of the linkage. These points in V may represent the intersection of two components of V, or may be the self-crossing of the same component. The surfaces are also tangent to each other when they touch in one point, which would lead to an isolated point in V. In addition, if a continuum of points of tangency is found, the surfaces are touching in a curve that is a component of $\mathcal{C}$.

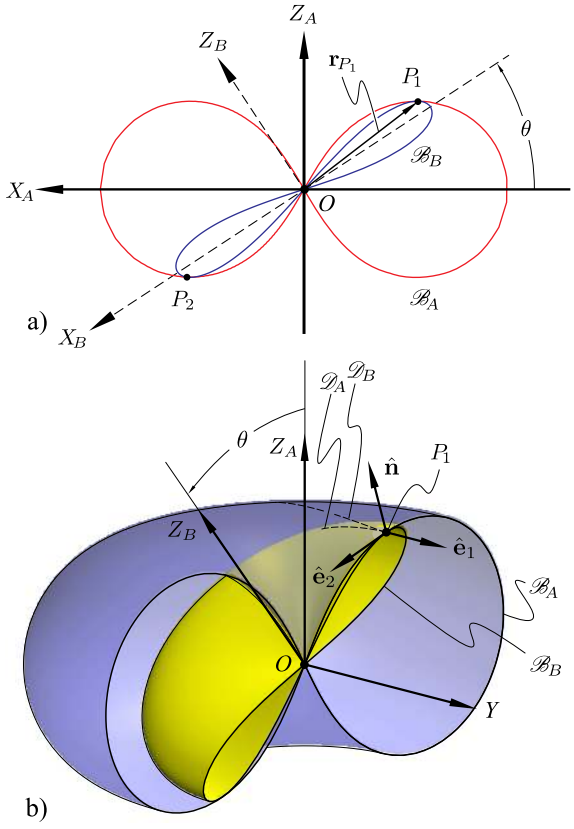

Fig. 5. Two singular toroids that are tangent to each other in the X_AZ_A plane.

To find the points where the intersection may become non-transverse, the real points $(x,y,z) \in \mathbb{R}^3$ that make $\nabla\phi_A(x,y,z) \times \nabla\phi_B(x,y,z) = \mathbf{0}$ and also satisfy $\phi_A(x,y,z) = \phi_B(x,y,z) = 0$ are explored. Two points in the Y axis are found, however, they imply $r_A = r_B$, so that the points are $(0,r_A,0) = (0,r_B,0)$ and $(0,-r_A,0) = (0,-r_B,0)$. This case leads to a linkage that is both line- and plane-symmetric. This example was analyzed before in [28] and the line-symmetric case was investigated by the authors of this paper in another work yet to be published. The other solutions that do not degenerate the toroids imply $y = 0$. Therefore, any point of tangency must lie in the X_AZ_A plane if the linkage is not the plane- and line-symmetric case. The solutions in the X_AZ_A plane are large expressions that involve not only

the construction parameters of the toroids, but also the angle θ. Considering the singular curves $\mathscr{B}_A$ and $\mathscr{B}_B$ obtained by $\mathscr{B}_i = \{(x,y) \in \mathbb{R}^2 \,|\, \phi_1(x,0,y) = 0\}$ (figure 5a), it is found that the curves become tangent to each other if:

$$\cos\theta = \pm \frac{\sqrt{(r_B^2\cos^2\gamma_B + r_A^2\sin^2\gamma_B)(r_A^2\cos^2\gamma_A + r_B^2\sin^2\gamma_A)}}{r_A r_B} \tag{8}$$

Each possibility leads to two solutions, therefore there are in total 4 values of θ that make the surfaces tanget to each other in the X_AY_A plane. Note that the argument of the square root is always positive, however, to obtain real values of θ, it is necessary that $(r_B^2\cos^2\gamma_B + r_A^2\sin^2\gamma_B)(r_A^2\cos^2\gamma_A + r_B^2\sin^2\gamma_A) \leq r_A^2 r_B^2$, since $\cos\theta \in [-1,1]$. After some algebra it is concluded that if $r_A > r_B$ then[3] $|\sin\gamma_B| > |\sin\gamma_A| \Rightarrow \sin\gamma_B^* > \sin\gamma_A^*$ and if $r_A < r_B$ then $|\sin\gamma_A| > |\sin\gamma_B| \Rightarrow \sin\gamma_A^* > \sin\gamma_B^*$. W.l.o.g. Fig. 5, shows the case in which $r_A > r_B \Rightarrow \sin\gamma_A^* > \sin\gamma_B^*$. This makes toroid B looking more flattened than toroid A.

6 Isolated points of tangency and Bricard structures.

The nature of the intersection when the two concentric singular toroids are tangent to each other in the X_AZ_A plane is now investigated. For this aim, consider the following proposition:

Proposition 6.1: The intersection of two concentric singular toroids with different radius contains only two isolated points if the toroids are tangent to each other at some point.

Proof: Let the two singular toroids to be intersected be $T^A_{r_A,r_A,\gamma_A,0}$ and $T^B_{r_B,r_B,\gamma_B,0}$, where $r_A \neq r_B$, thus the only possibility for tangent intersection is that the surfaces are tangent to each other in the X_AZ_A plane. Replacing the values of θ from Eq. (8) in the parameterizations of the surfaces and trying to find $\mathcal{C}$ would lead to quite complicated expressions. A simpler way to proceed is to analyze the normal curvatures of the toroids in one of the points where the surfaces are tangent. The normal curvatures of both surfaces must be the same in the direction that is tangent to the intersection curve. If there is no intersection curve and the surfaces are only touching in such point, the curvatures are always different for both surfaces in any direction. Since normal curvature is invariant to frame transformations both toroids can be analyzed in their own coordinate systems. According to Euler's formula, the normal curvature is given by: $\kappa(\psi) = \kappa_1\cos^2\psi + \kappa_2\sin^2\psi$, where κ_1 and κ_2 are the curvatures in the principal directions $\hat{\mathbf{e}}_1$ and $\hat{\mathbf{e}}_2$ and ψ is the angle that defines the direction of the normal curvature with respect to one of the principal directions.

The singular toroids are surfaces of revolution with $\mathscr{B}$ being rotated about the Z axis. It is known (see for example [46]) that in surfaces of revolution the principal curvatures are the tangents to the meridian and parallel crossing the point in analysis. Hence, for the arrangement shown in Fig. 5b $\hat{\mathbf{e}}_1 = \hat{\mathbf{j}}$ and $\hat{\mathbf{e}}_2 = \hat{\mathbf{t}}$, where $\hat{\mathbf{t}}$ is the mutual tangent vector to $\mathscr{B}_A$ and $\mathscr{B}_B$ at P_1. If the intersection includes a curve crossing P_1, it should be possible to find an angle $\psi \in \mathbb{T}$, such that:

$$\begin{aligned} \kappa_{1A}\cos^2\psi + \kappa_{2A}\sin^2\psi &= \kappa_{1B}\cos^2\psi + \kappa_{2B}\sin^2\psi \\ \Leftrightarrow \frac{\kappa_{1A} - \kappa_{1B}}{\kappa_{2B} - \kappa_{2A}} &= \tan^2\psi \geq 0 \end{aligned} \tag{9}$$

where κ_{iA} and κ_{iB}, $i = 1,2$, are the principal curvatures at P_1 of toroids A and B, respectively. From Fig. 5b Note that κ_{2j}, $j = A,B$ are the curvatures of plane curves $\mathscr{B}_j$, while κ_{1j} are the curvatures of plane curves $\mathscr{D}_j$ obtained by intersecting the toroids with the plane that contains P_1 and is spanned by $\hat{\mathbf{e}}_1 = \hat{\mathbf{j}}$ and $\hat{\mathbf{n}}$. If, w.l.o.g. $r_A > r_B$ as shown in Fig. 5, it is clear that $\kappa_{2B} > \kappa_{2A}$ and $\kappa_{2B} - \kappa_{2A} > 0$. Hence, in order to have a real solution of Eq. (9), it is necessary that $\kappa_{1A} - \kappa_{1B} > 0$. These curvatures can be computed using the following expression [47]:

$$\kappa_{1j} := \kappa(\phi_j, \hat{\mathbf{j}})(P_1) = \left.\frac{\hat{\mathbf{j}}^T \mathrm{Hess}(\phi_j(x,y,z))\hat{\mathbf{j}}}{|\nabla\phi_j(x,y,z)|}\right|_{(x,y,z)=P_1}, \; j = A,B$$

where, $\mathrm{Hess} : \mathbb{R}[x,y,z] \to M^{3\times3}(\mathbb{R})$ is the Hessian matrix of the given implicit form. Upon calculations it is concluded that:

$$\kappa_{1j} = \frac{|\sin\gamma_j|(|\mathbf{r}_{P_1}|^2 - 2r_j^2)}{2|\mathbf{r}_{P_1}|r_j\sqrt{|\mathbf{r}_{P_1}|^2 - 2(|\mathbf{r}_{P_1}|^2 - 2r_j^2)\cos^2\gamma_j}}, \; j = A,B \tag{10}$$

where $|\mathbf{r}_{P_1}|$,is the magnitude of the position vector of P_1, which is the same value for both toroids and is invariant to frame transformations. $|\mathbf{r}_{P_1}|$ is calculated using the value of θ in Eq. (8), leading to:

$$|\mathbf{r}_{P_1}| = 2\sqrt{\frac{r_B^4\sin^2\gamma_A\cos^2\gamma_B - r_A^4\sin^2\gamma_B\cos^2\gamma_A}{r_B^2\sin^2\gamma_A\cos^2\gamma_B - r_A^2\sin^2\gamma_B\cos^2\gamma_A + (r_A^2 - r_B^2)\sin^2\gamma_A\sin^2\gamma_B}}$$

Replacing this value in Eq. (10) and carrying out simplifications it can be concluded that, $\kappa_{1A} - \kappa_{1B}$ has the same sign as $r_B - r_A$. Therefore, if $r_A > r_B$ (as first supposed for this proof), $\kappa_{1A} - \kappa_{1B} < 0$, $\tan^2\psi < 0 \Rightarrow \psi \notin \mathbb{T}$ and there is no real solution for Eq. (9). Hence, both toroids are touching each other in P_1 and P_2 but these are isolated points in $\mathcal{C} = \{P_1, P_2, O\}$. ■

Two important conclusions can be drawn from the previous proposition: First, a Bricard linkage fulfilling the plane symmetry conditions can be a 0-DOF structure which can be assembled in two different configurations. However, if the linkage is assembled in $E(\mathbf{q}) = O$ the same linkage has 1 DOF and works as a spherical 4R linkage. In such case, V is composed of 3 regions: 2 isolated points and a 1-dimensional curve in $\mathbb{T}^6$. And second, there is no way to reconfigure these

[3] The same toroid can be generated using different angles γ, [44]. From these, we take γ^* in $(0,\pi/2]$, which is unique for any toroid.

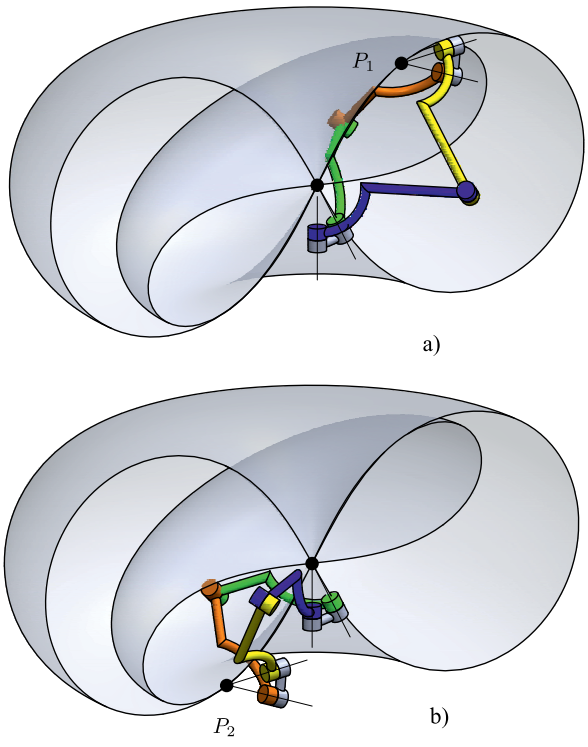

Fig. 6. A Bricard plane-symmetric linkage with finite mobility zero in its two different assembly modes.

linkages directly from one curve to another at least the linkage is also line-symmetric.

As an example of this situation, consider the plane-symmetric linkage with the following DH parameters:

$$\begin{aligned} &\alpha_{A1,A2} = \tfrac{4}{3}\pi, \ \alpha_{B2,B1} = \tfrac{5}{6}\pi, \ \alpha_{B1,A1} = \arccos\left(\tfrac{247}{280}\right), \\ &a_{A1,A2} = 10, \ a_{B2,B1} = 7, \ a_{B1,A1} = 0 \\ &\alpha_{A2,A3} = \tfrac{2}{3}\pi, \ \alpha_{B3,B2} = \tfrac{7}{6}\pi, \ \alpha_{A3,B3} = -\arccos\left(\tfrac{247}{280}\right), \\ &a_{A2,A3} = 10, \ a_{B3,B2} = 7, \ a_{A3,B3} = 0 \end{aligned} \tag{11}$$

and $d_i = 0$ for all joints. These parameters satisfy the conditions in Eqs. (1) and (4) and, therefore, the linkage is plane-symmetric and it generates the intersection of two concentric singular toroids. From these parameters it can be seen that $\gamma_A^* = \frac{1}{3}\pi$, $r_A = 10$, $\gamma_B^* = \frac{1}{6}\pi$, $r_B = 7$ and $\theta = \arccos\left(\frac{247}{280}\right)$, which turns out to be one of the 8 values that can be obtained from Eq. 8. Thus, the Bricard linkage must be a structure with 0 DOF if assembled in any of the two isolated points. If assembled with $E = O$ the linkage should behave as a spherical 4-bar linkage, however, observe that such spherical linkage would have twist angles $2\gamma_A = \frac{2}{3}\pi$, $2\gamma_B = \frac{1}{3}\pi$ and two links with angles $\arccos\left(\frac{247}{280}\right)$, the largest angle is $\frac{2}{3}\pi$ but $\frac{2}{3}\pi > \frac{1}{3}\pi + 2\arccos\left(\frac{247}{280}\right)$, therefore the spherical linkage cannot be assembled. The only two possible assembly modes are those for which the linkage is a structure, namely $E(\mathbf{q}_1) = P_1$ and $E(\mathbf{q}_2) = P_2$, these are presented in figure 6.

Consider the linkage assembled in an isolated point $E(\mathbf{q}_1) = P_1$ in figure 8, some interesting results regarding the reciprocal system of the screw system of the linkage are now obtained: First, the plane of symmetry is perpendicular to and bisects the segment OE, which lies on the X_AZ_A plane, thus the plane of symmetry is perpendicular to the X_AZ_A plane. As a consequence of this, S_{A3} and S_{B3} lie on the plane X_AZ_A, since their symmetric members, S_{A1} and S_{B1} lie on X_AZ_A which is perpendicular to the plane of symmetry. Then, the axis of the special linear complex is the intersection of the plane of symmetry and the X_AZ_A plane as expected from Section 2.

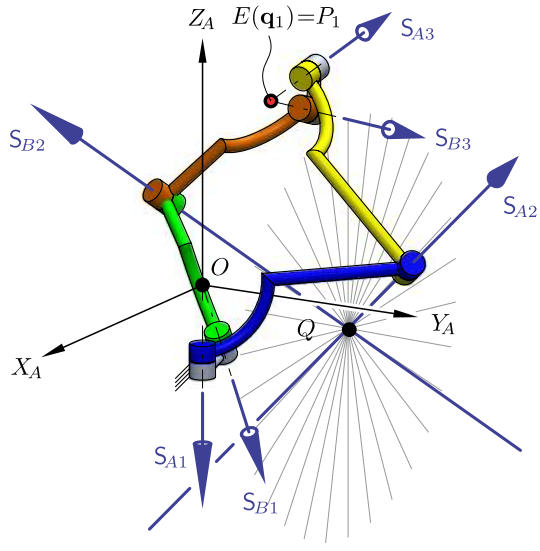

Fig. 7. A Bricard plane-symmetric linkage with finite mobility zero in the assembly mode with $E(\mathbf{q}_1) = P_1$.

Knowing the value of θ, it is possible to calculate both u_A and u_B for any of the two configurations in which the linkage can be assembled without using the double singularity and making it a spherical 4R linkage. With u_A and u_B, the following Plücker coordinates are obtained for the screws $A2$ and $B2$, respectively:

$$\begin{aligned} {}^A\mathsf{S}_{A2}(\mathbf{q}_1) = \Bigg(&\frac{3\sqrt{17391}}{682}, \frac{\sqrt{48081}}{341}, \frac{1}{2}; \frac{15\sqrt{5797}}{341}, \\ &\frac{10\sqrt{16027}}{341}, -5\sqrt{3} \Bigg), \\ {}^A\mathsf{S}_{B2}(\mathbf{q}_1) = \Bigg(&\frac{63\sqrt{5797}}{6820}, \frac{\sqrt{16027}}{341}, \frac{7\sqrt{3}}{20}; \frac{5\sqrt{17391}}{341}, \\ &\frac{7\sqrt{48081}}{341}, -5 \Bigg). \end{aligned}$$

Previously, it was proved that S_{A2} and S_{B2} always intersect. If the screws are defined by $\mathsf{S}_i = (\hat{\mathbf{s}}_i; \mathbf{m}_i)$, $i = A2, B2$, such intersection point is given by $P = (\hat{\mathbf{s}}_{A2} \cdot \mathbf{m}_{B2})^{-1}\mathbf{m}_{A2} \times \mathbf{m}_{B2}$. However, it turns out that for this example $({}^A\mathbf{m}_{A2} \times {}^A\mathbf{m}_{B2}) \cdot {}^A\mathbf{j} = 0$, which means that P lies on the X_AZ_A plane. This implies that a pencil of lines in the X_AZ_A plane can be

drawn with center in P and each line in the pencil will be reciprocal to all the axes of the linkage. Hence, the reciprocal system is a 2-system and the first order mobility of the linkage is 2. A velocity analysis applied to this structure would reveal that the linkage has 2 degrees of freedom since the tangent space of V in such configuration is a 2-dimensional space. A tangent cone [48, 49, 50, 51, 52, 23] analysis was made for this configuration. While the first order approximation is a 2-dimensional vector space, as expected, the second order approximation is 0-dimensional, proving that the linkage is actually a structure. It is then said that the structure has second order rigidity [53].

7 Motion branch reconfiguration through the double singularity.

Reconfiguration of motion branches can be achieved using the double singularity of the concentric toroids if there are curves crossing it. Due to the symmetry of the intersection, and since there are no points of tangency (excluding the known exceptions), it can be concluded that the intersection will have any of the following forms:

1. Two regular disjoint curves and the double singularity point
2. One singular 8-shaped curve with its self-crossing coincident with the double singularity,
3. Two singular 8-shaped curves that share the same self-crossing point which is coincident with the double singularity.

The first case is generated by non-reconfigurable linkages since there is no way to migrate from one curve to another or to visit the double singularity. The second case is reconfigurable with two motion branches: a Bricard 6R operation mode and a spherical 4R linkage mode. The third case is the most interesting since the configuration space includes two Bricard branches which can be visited by the linkage without disassembling it and, in addition, the linkage can undergo spherical 4R motion branches.

In figure 8, note that if in the X_AZ_A plane $\mathscr{B}_A \cap \mathscr{B}_B = \{O\}$ the intersection of the toroids includes two singular curves as in the third case of intersection. Since the toroids are symmetric with the X_AZ_A plane, if $\mathscr{B}_B$ crosses $\mathscr{B}_A$ in four points, the intersection curve never includes O, as in the first case of intersection. If $\mathscr{B}_B$ crosses $\mathscr{B}_A$ in two points, the intersection curve crosses O and then intersects the X_AZ_A plane in the two points where $\mathscr{B}_B$ crosses $\mathscr{B}_A$, the intersection of toroids is then a sole singular curve, as in the second case of intersection. Now imagine that the two points where the intersection crosses the X_AZ_A move through $\mathscr{B}_A$ approaching O, since the intersection is symmetric with the X_AZ_A plane, the curve starts to sharpen in such points until they reach O and the intersection becomes two singular curves. Refer to figure 8a, it is easy to prove that the tangent to $\mathscr{B}_i$, $i = A, B$ makes an angle γ_i^* with the x_i axis. Then the conditions that

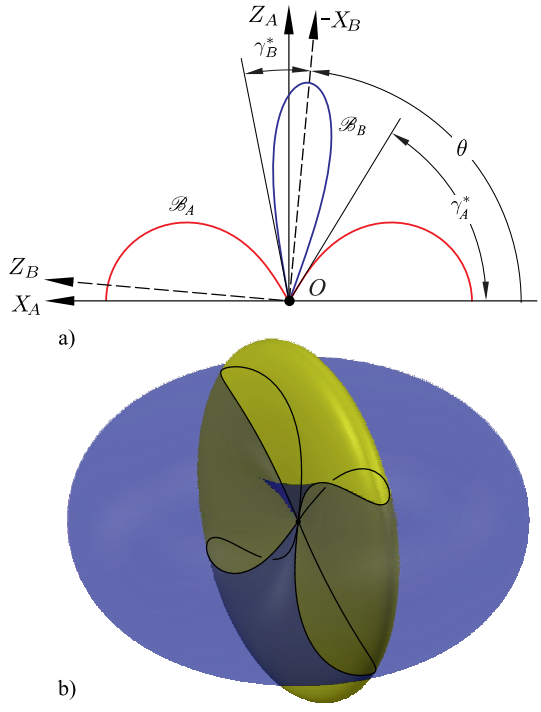

Fig. 8. A case with two singular curves in the intersection: a) $\mathscr{B}_A$ and $\mathscr{B}_B$ curves, b) surfaces and intersection.

make $\mathscr{B}_B$ intersect $\mathscr{B}_A$ only in O are the following:

$$\begin{aligned} \gamma_A^* + \gamma_B^* &< \frac{\pi}{2} \\ \gamma_A^* + \gamma_B^* &< \theta < \pi - \gamma_A^* - \gamma_B^* \end{aligned} \tag{12}$$

In the remaining part of the paper we focus exclusively in linkages whose generated toroids fulfill conditions 12, since these are the most complicated cases.

8 Bricard branches as a link between crank-rocker spherical 4R branches.

Let $\mathcal{C} = \mathscr{C}_1 \cup \mathscr{C}_2$, like in the third case of intersection, then $\mathscr{C}_1 \cap \mathscr{C}_2 = \{O\}$. it has to be considered that, even though the two curves intersect in one point, if V_i is the component of V related to $\mathscr{C}_i$, then $V_1 \cap V_2 = \emptyset$, which means that the linkage cannot reconfigure from V_1 to V_2 directly. This is a consequence of the double-singularity O. In any regular point in a surface all curves intersecting the point do it with the same values of $(u, v) \in U$, as σ is a bijection from U to $\mathcal{S} \setminus \text{sing}(\mathcal{S})$. But since in the conic singularity of the singular toroids $\partial\sigma/\partial u = \mathbf{0}$ there are an infinity of pairs (u, v) that map to O and the only way to escape from the singularity is moving in the direction of the isoparametric curve of v, since $\partial\sigma/\partial v \neq \mathbf{0}$ is such point. These isoparametric curves are the secondary circles, their tangent vectors in the singularity generate a cone that is tanget to the toroid in the singularity. Any two curves on the toroid crossing the singularity with non-parallel tangent vectors at O will have different values $(u(t), v(t))$ at O, since they reached the point in different secondary circles.

The previous paragraph implies that in general the linkage cannot move from V_1 to V_2 since E reaches O in different configurations. In fact, in the self-crossing of each singular curve in $\mathcal{C}$, the linkage is unable to chose between the two segments in the neighborhood of O, E smoothly passes the double singularity and V_1 and V_2 are free of singularities even though they are related to singular curves $\mathscr{C}_1$ and $\mathscr{C}_2$. Despite V_1 and V_2 are disjoint, they are connected through the spherical 4R motion branch related to the double singularity. For the evolved spherical 4R linkage two opposite links have the same twist angle, θ, while the other two links have twist angles $2|\gamma_A|$ and $2|\gamma_B|$.

Suppose E lies on $\mathscr{C}_1$ and approaches O, once the linkage starts working in the spherical 4R branch axes S_{A2} and S_{B2} can move until the secondary circles are both tangent to $\mathscr{C}_2$ and E can scape from the double singularity allowing the linkage to enter the V_2 branch. Since there are two singular curves crossing O, there are in total four different directions in which E can move to scape from O. Two of these will reconfigure a spherical 4R branch into the same plane-symmetric Bricard branch related to $\mathscr{C}_1$, while the other two will reconfigure to the branch related to $\mathscr{C}_2$. In each of these configurations the evolved spherical 4R linkage most be in a plane-symmetric configuration since such configuration also belongs to a Bricard branch. Fig. 9 shows a plane-symmetric linkage in a spherical 4R branch with $E = O$, the linkage is about to scape to V_1 since the secondary circles C_{2A} and C_{2B} are both tangent to $\mathscr{C}_1$ at O.

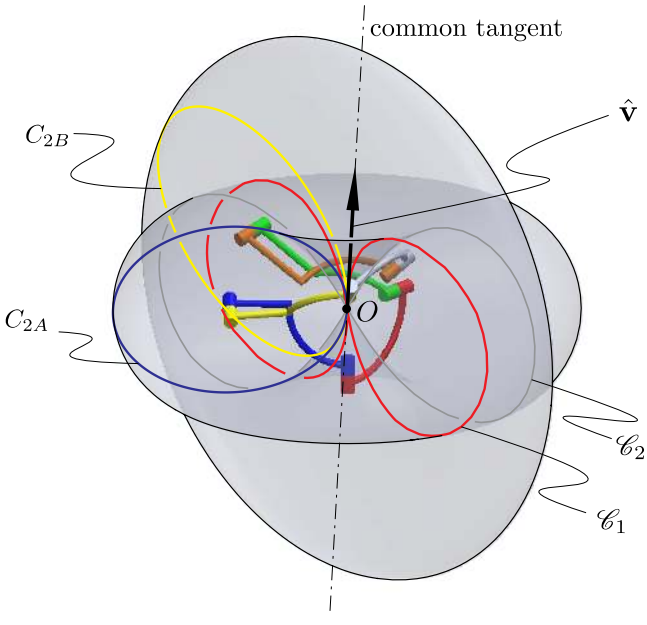

Fig. 9. A reconfigurable Bricard plane-symmetric linkage in its spherical 4R operation mode, with its two secondary circles tangent to each other and to curve $\mathscr{C}_1$ and the linkage is about to escape to V_1.

.

However, it is known that the configuration space of the spherical 4R linkages may include two branches which may or may not intersect. It is possible that the two configurations that allow to scape to V_1 (E scaping from O to $\mathscr{C}_1$) belong to the same branch of the 4R linkage, while the other two configurations to scape to V_2 (E scaping from O to $\mathscr{C}_2$) belong to the other branch of the 4R linkage. In such case, in order to reconfigure the linkage from V_1 to V_2 it is necessary to disassemble it if the two spherical 4R branches are disjoint. Therefore, the following paragraphs investigate the two spherical 4R branches and the four scape configurations in order to establish the restrictions that ensure that the linkage can reconfigure through all of its branches. We begin by analyzing the rotability of the evolved spherical 4R linkages since branch identification is different depending on the rotability of the links. However, we restrict this analysis to the cases in which the toroid generators are built using $|\gamma| = \gamma^*$

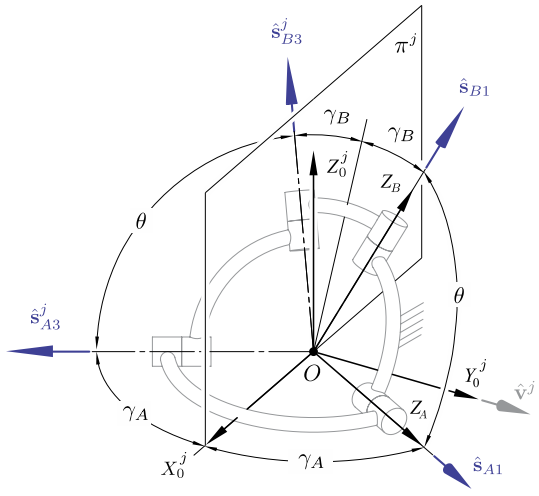

Fig. 10. A plane-symmetric configuration of a spherical 4R linkage with two opposite links of the same angle.

.

Proposition 6.1: The spherical 4R linkages obtained as a behavior of Bricard plane-symmetric linkages that generate two concentric toroids intersecting in two curves are either crank-rocker or change-point.

Proof: Let the twist angles of the spherical four-bar linkage evolved from the Bricard plane-symmetric linkage be $\alpha_{A1,A3} = 2|\gamma_A|$, $\alpha_{A3,B3} = \alpha_{B1,A1} = \theta$ and $\alpha_{B3,B1} = 2|\gamma_B|$ (Fig. 10). From the second condition in Eq. (12): $\theta + \gamma_A + \gamma_B < \pi \Rightarrow 2\theta + 2\gamma_A + 2\gamma_B < 2\pi$, then $\Sigma\alpha_i < 2\pi$. According to Gupta and Ma [54], if the sum of twist angles is less that 2π, the full rotability criterion is quite similar to that for the planar case: if $\alpha_{\min} + \alpha_{\max} < \alpha_p + \alpha_q$, then at least one of the links is fully rotatable.

From the second condition in Eq. (12), $\gamma_A + \gamma_B < \theta \Rightarrow \frac{1}{2}(\alpha_{A1,A3} + \alpha_{B3,B1}) < \alpha_{A3,B3} = \alpha_{B1,A1}$ and $\alpha_{\min} \neq \alpha_{A3,B3} = \alpha_{B1,A1}$. By contradiction consider that none of the links is fully rotatable. Then, if $\alpha_{\max} = \alpha_{A3,B3} = \alpha_{B1,A1} = \theta$, from the criterion it follows:

$$\alpha_{\min} + \theta > \theta + \alpha_q \Rightarrow \alpha_{\min} > \alpha_q$$

which is a contradiction. In a similar way, now consider $\alpha_p = \alpha_q = \alpha_{A3,B3} = \alpha_{B1,A1} = \theta$:

$$\alpha_{\min} + \alpha_{\max} > 2\theta \Rightarrow \alpha_{A1,A3} + \alpha_{B3,B1} > 2\theta$$

which contradicts the second condition in Eq. (12). Hence, it is proved that at least one of the links is fully rotatable. This link is the one whose twist angle is $\alpha_{\min}$. In Fig. 10 it can be seen that the twist angle for the coupler and fixed links is θ, which is proved to be different to $\alpha_{\min}$. Therefore, the smallest twist angle corresponds to either the input or output links. Hence, all the linkages are crank-rocker or, if $\alpha_{A1,A3} = \alpha_{B3,B1} \Rightarrow \gamma_A = \gamma_B$, change-point. ■

It is known [55] that in crank-rocker (or rocker-crank) 4R linkages both branches are disjoint. Therefore, from Proposition 6.1 it is concluded that the only way to have a special configuration joining the two branches is the spherical equivalent of a parallelogram linkage. In such a very special case the criterion for branch change is simply the parallel- or anti-parallelism of the links. For crank-rockers (or rocker-cranks), the following two propositions allow the identification of branch change.

Proposition 6.2: A 4R linkage with two opposite links of the same twist angle can reach four plane-symmetric configurations, two of them belong to the same branch while the other two belong to the other branch.

Proof: Refer to Fig. 10, which shows the spherical 4R linkage with two opposite links of the same twist angle, θ, the angle of the other two links are $2\gamma_A$ and $2\gamma_B$. The linkage is shown in a plane-symmetric configuration. $\hat{\mathbf{s}}_{A1}$, $\hat{\mathbf{s}}_{A3}$, $\hat{\mathbf{s}}_{B3}$ and $\hat{\mathbf{s}}_{B1}$ are the unit vectors parallel to the axes of the revolute joints. A coordinate system $X_0Y_0Z_0$ is placed fixed to the symmetry plane π, so that π coincides with the plane X_0Z_0 and X_0 bisects the angle between $\hat{\mathbf{s}}_{A1}$ and $\hat{\mathbf{s}}_{A3}$.

The linkage is symmetric with respect to π when ${}^0\hat{\mathbf{s}}_{i1} \cdot \hat{\mathbf{j}} = -{}^0\hat{\mathbf{s}}_{i3} \cdot \hat{\mathbf{j}}$ while ${}^0\hat{\mathbf{s}}_{i1} \cdot \hat{\mathbf{i}} = {}^0\hat{\mathbf{s}}_{i3} \cdot \hat{\mathbf{i}}$ and ${}^0\hat{\mathbf{s}}_{i1} \cdot \hat{\mathbf{k}} = {}^0\hat{\mathbf{s}}_{i3} \cdot \hat{\mathbf{k}}$, $i = A,B$. Adding this restriction, the following four solutions are found for ${}^0\hat{\mathbf{s}}_{B1}$:

$$
\begin{aligned}
{}^0\hat{\mathbf{s}}^1_{B1} &= \left(\frac{\cos\theta}{\cos\gamma_B} - \frac{K_1}{2\cos^2\gamma_B}, \frac{K_1}{\cos\gamma_B \sin\gamma_B}, \sqrt{\frac{K_2 + K_1\cos\theta}{\cos^3\gamma_B}} \right) \\
{}^0\hat{\mathbf{s}}^2_{B1} &= \left(\frac{\cos\theta}{\cos\gamma_B} - \frac{K_1}{2\cos^2\gamma_B}, \frac{K_1}{\cos\gamma_B \sin\gamma_B}, -\sqrt{\frac{K_2 + K_1\cos\theta}{\cos^3\gamma_B}} \right) \\
{}^0\hat{\mathbf{s}}^3_{B1} &= \left(\frac{\cos\theta}{\cos\gamma_B} + \frac{K_1}{2\cos^2\gamma_B}, -\frac{K_1}{\cos\gamma_B \sin\gamma_B}, \sqrt{\frac{K_2 - K_1\cos\theta}{\cos^3\gamma_B}} \right) \\
{}^0\hat{\mathbf{s}}^4_{B1} &= \left(\frac{\cos\theta}{\cos\gamma_B} + \frac{K_1}{2\cos^2\gamma_B}, -\frac{K_1}{\cos\gamma_B \sin\gamma_B}, -\sqrt{\frac{K_2 - K_1\cos\theta}{\cos^3\gamma_B}} \right)
\end{aligned}
\tag{13}
$$

where $K_1 = |\cos\gamma_B \sin\gamma_B| \sqrt{2(1-\cos\gamma_A)}$ and $K_2 = \frac{1}{2}\cos\gamma_B(2\cos^2\gamma_B - 2\cos^2\theta + \cos\gamma_A - 1)$. ${}^0\hat{\mathbf{s}}^k_{B3}$, $k = 1,\ldots,4$ can be obtained from ${}^0\hat{\mathbf{s}}^k_{B1}$ by simply changing the sign of the Y_0 component of each vector. ${}^0\hat{\mathbf{s}}_{A1}$ and ${}^0\hat{\mathbf{s}}_{A3}$ are the same for all configurations since they are fixed to plane π.

According to [56], if the linkage is crank-rocker (or rocker-crank), all the configurations for which $\eta_k := {}^0\hat{\mathbf{s}}_{A1} \times {}^0\hat{\mathbf{s}}^k_{B3} \cdot {}^0\hat{\mathbf{s}}^k_{A3}$ has the same sign belong to the same branch. Upon calculation it is found that, $\text{sign}(\eta_1) = \text{sign}(\eta_3) = \text{sign}(\cos\gamma_B \sin\gamma_B)$ and $\text{sign}(\eta_2) = \text{sign}(\eta_4) = -\text{sign}(\cos\gamma_B \sin\gamma_B)$. Hence, it is concluded that plane-symmetric configurations 1 and 3 lie in the same branch, while configurations 2 and 4 lie in the other branch. ■

From Proposition 6.2 it can be seen that the two different Bricard branches may reconfigure to spherical 4R modes in different branches, making impossible to move from one Bricard branch to the other. Each of the four plane-symmetric configurations presented in Proposition 6.2 is a bifurcation configuration between Bricard branches and spherical 4R branches. Therefore, a vector $\hat{\mathbf{v}}^j$ tangent to the curve of intersection at O can be calculated for each of these configurations. For the sake of simplicity we call these vectors *escape directions*

Proposition 6.3 Given a plane-symmetric Bricard linkage generated from the intersection of two concentric singular toroids with the axis of one rotated about the Y axis from the other, the escape directions lying on the same side of the plane XZ correspond to configurations lying in the same spherical 4R branch.

Proof: From the geometry of the plane-symmetric linkages obtained from the intersection of two concentric singular toroids it can be proved that the escape directions $\hat{\mathbf{v}}_j$ are parallel to[4] $(\hat{\mathbf{s}}_{B3} \times \hat{\mathbf{s}}_{B1}) \times (\hat{\mathbf{s}}_{A3} \times \hat{\mathbf{s}}_{A1}) || \hat{\mathbf{j}}_0$, where $\hat{\mathbf{j}}_0$ is the unit vector in the direction of Y_0 in Fig. 10. Each of the four configurations obtained in Proposition 6.2 lead to a escape direction $\hat{\mathbf{v}}_j$. We are interested in obtaining such vectors in the coordinate system A, which is fixed, while coordinate system 0 moves from one configuration to another. Therefore, for coordinate system A, vectors ${}^A\hat{\mathbf{s}}_{A1}$ and ${}^A\hat{\mathbf{s}}_{B1}$ are fixed, while there are four sets of vectors ${}^A\hat{\mathbf{s}}^j_{A3}$ and ${}^A\hat{\mathbf{s}}^j_{B3}$.

The escape directions are calculated by finding the bases $\left\{ {}^0\hat{\mathbf{i}}^j_A, {}^0\hat{\mathbf{j}}^j_A, {}^0\hat{\mathbf{k}}^j_A \right\}$:

$${}^A\hat{\mathbf{v}}_j = {}^A\hat{\mathbf{j}}^j_0 = {}^A_0\mathbf{T}_j \, {}^0\hat{\mathbf{j}}_0 = \text{aug}\left({}^0\hat{\mathbf{i}}^j_A, {}^0\hat{\mathbf{j}}^j_A, {}^0\hat{\mathbf{k}}^j_A \right)^{-1} \hat{\mathbf{j}}$$

The following four escape directions are found, each related to each of the symmetric configurations found in Propo-

[4] The radius of the secondary circles are the common perpendiculars between axes S_{i1} and S_{i2}, $i = A,B$. In the spherical 4R branches this line segment coincides with the common perpendicular of S_{i2} and S_{i3}. Therefore, $\hat{\mathbf{s}}_{i1} \times \hat{\mathbf{s}}_{i3}$ must be parallel to the radius of C_{2i}. Since the circles are tangent to each other in the escape configurations and this tangent is perpendicular to the radii of both circles, it follows that the tangent is parallel to $(\hat{\mathbf{s}}_{B3} \times \hat{\mathbf{s}}_{B1}) \times (\hat{\mathbf{s}}_{A3} \times \hat{\mathbf{s}}_{A1})$

sition 6.2:

$$
{}^{A}\hat{\mathbf{v}}_1 = \left(\frac{-2\cos\theta\cos\gamma_B\sin^2\gamma_B + K_1}{2|\sin\theta|\cos\gamma_B\sin\gamma_B}, -\frac{\cos\gamma_B\sqrt{2K_2+K_1}}{|\sin\theta|\sqrt{\cos^3\gamma_B}}, \sin\gamma_B \right)
$$

$$
{}^{A}\hat{\mathbf{v}}_2 = \left(\frac{-2\cos\theta\cos\gamma_B\sin^2\gamma_B + K_1}{2|\sin\theta|\cos\gamma_B\sin\gamma_B}, \frac{\cos\gamma_B\sqrt{2K_2+K_1}}{|\sin\theta|\sqrt{\cos^3\gamma_B}}, \sin\gamma_B \right)
$$

$$
{}^{A}\hat{\mathbf{v}}_3 = \left(\frac{-2\cos\theta\cos\gamma_B\sin^2\gamma_B - K_1}{2|\sin\theta|\cos\gamma_B\sin\gamma_B}, -\frac{\cos\gamma_B\sqrt{2K_2-K_1}}{|\sin\theta|\sqrt{\cos^3\gamma_B}}, \sin\gamma_B \right)
$$

$$
{}^{A}\hat{\mathbf{v}}_4 = \left(\frac{-2\cos\theta\cos\gamma_B\sin^2\gamma_B - K_1}{2|\sin\theta|\cos\gamma_B\sin\gamma_B}, \frac{\cos\gamma_B\sqrt{2K_2-K_1}}{|\sin\theta|\sqrt{\cos^3\gamma_B}}, \sin\gamma_B \right)
$$

It can be seen that ${}^{A}\hat{\mathbf{v}}_1$ and ${}^{A}\hat{\mathbf{v}}_2$ (${}^{A}\hat{\mathbf{v}}_3$ and ${}^{A}\hat{\mathbf{v}}_4$) are symmetric with respect to the X_AZ_A plane as the only difference between them is the sign of the Y component. The sign of the Y components of ${}^{A}\hat{\mathbf{v}}_1$ and ${}^{A}\hat{\mathbf{v}}_3$ (${}^{A}\hat{\mathbf{v}}_2$ and ${}^{A}\hat{\mathbf{v}}_4$) is the same, namely $-\text{sign}(\cos\gamma_B)$ ($\text{sign}(\cos\gamma_B)$), hence they lie in the same side of the X_AZ_A plane. In addition, all these vectors lie in the same side of the X_AY_A plane as their Z components are the same, namely $-\text{sign}(\sin\gamma_B)$. From Proposition 6.2 it is known that configurations 1 and 3 (2 and 4) lie in the same branch, therefore it can be concluded that the escape directions lying in the same side of the X_AZ_A plane belong to the same branch of the spherical 4R linkage. ■

Fig. 11 shows three possible cases of intersection composed by two curves: $r_A > r_B$, $r_A = r_B$ and $r_A < r_B$. In each case the tangent vector to the curves at O, the double singularity point, are shown. These tangent vectors are the same that were calculated in Proposition 6.3, in which it was proven that if these 4 vectors have Z_A component of the same sign, then: when the vectors lie in the same side of the X_AZ_A plane the configurations of the spherical 4R linkage lie in the same branch. From Fig. 11 it can be seen that for the case $r_A > r_B$ the vectors lying on the same side of the X_AZ_A plane are tangent to the same curve, and since these configurations belong to the same spherical 4R branch reconfiguration to the other curve is impossible and the two spherical 4R branches cannot be reached without disassembling the linkage. For $r_A = r_B$ and $r_A < r_B$ the two vectors lying on the same side of the X_AZ_A are tangent to different curves, this means that it is possible to reconfigure the disjoint spherical 4R branches without disassembling the linkage as both branches are connected through a Bricard branch related to each of the two curves.

It can be proved[5] that for the change-point evolved spherical 4R linkages the escape directions that are symmetric with respect to the plane X_AZ_A belong to the same branch. Therefore, from Fig. 11, if $r_A > r_B$ the same Bricard branch can be reconfigured to parallel or anti-parallel branches of change-point spherical 4R linkage.

Fig. 12 shows the reconfiguration diagrams for two cases of reconfigurable plane-symmetric linkage obtained from the toroids intersection. The diagram in Fig. 12a is related to a case with two crank-rocker spherical 4R branches, it is known that these branches are disjoint, but it is possible to reach both branches without disassembling the linkage since they are communicated through two different Bricard plane-symmetric branches. Fig. 12b shows a more complicated case in which $r_A = r_B$ and $|\gamma_A| = |\gamma_B|$, leading to a plane- and line-symmetric linkage for which the toroids are tangent to each other in two points in the Y axis, these singularities communicate the two Bricard branches, furthermore, since $|\gamma_A| = |\gamma_B|$ the evolved spherical 4R linkage is change-point, allowing a direct reconfiguration between its two branches through the special configuration.

9 An example with two spherical 4R branches connected through two Bricard plane-symmetric branches.

Consider the plane-symmetric linkage shown in figure 13 which has the following DH parameters:

$$
\begin{array}{lll}
\alpha_{A1,A2} = \frac{1}{3}\pi, & \alpha_{B2,B1} = \frac{23}{12}\pi, & \alpha_{B1,A1} = \frac{17}{36}\pi, \\
a_{A1,A2} = 5, & a_{B2,B1} = 6, & a_{B1,A1} = 0 \\
\alpha_{A2,A3} = \frac{5}{3}\pi, & \alpha_{B3,B2} = \frac{1}{12}\pi, & \alpha_{A3,B3} = \frac{55}{36}\pi, \\
a_{A2,A3} = 5, & a_{B3,B2} = 6, & a_{A3,B3} = 0
\end{array}
\tag{14}
$$

then the linkage generates the intersection of two concentric singular toroids, such that $\gamma_A = \frac{1}{3}\pi$, $r_A = 5$, $\gamma_B = -\frac{15}{180}\pi$, $r_B = 6$ and $\theta = \frac{85}{180}\pi$. These construction parameters satisfy the conditions in Eq. 12, therefore $\mathcal{C} = \mathscr{C}_1 \cup \mathscr{C}_2$ such that $\mathscr{C}_1 \cap \mathscr{C}_2 = \{O\}$. Since E can reach the double singularity O the linkage has four motion branches: two Bricard branches and two spherical 4R branches. In addition, since $r_A < r_B$ and $\gamma_A \neq \gamma_B$ the linkage should be able to move through the two spherical 4R branches without disassembling it.

Figure 14 shows the linkage in several configurations in each motion branch. Observe that the two configurations belonging to V_1 (V_2) for which $E = O$ are different as expected. None of these four symmetric configurations coincide since V_1 and V_2 are disjoint. However, each of these is singular in V, allowing the reconfiguration to V_{O1} and V_{O2}, the spherical 4R branches, for which $E(\mathbf{q}) = O$, $\forall \mathbf{q} \in V_{O1} \cup V_{O2}$. The reconfiguration between branches is presented in the diagram in Fig. 12a, which shows how the two branches of the evolved spherical 4R linkage are connected through plane-symmetric Bricard branches allowing reconfigurability without disassembling.

[5] Such a proof, as mentioned above, is based on the parallelism or anti-parallelism of the links. The proof is not presented due to space reasons.

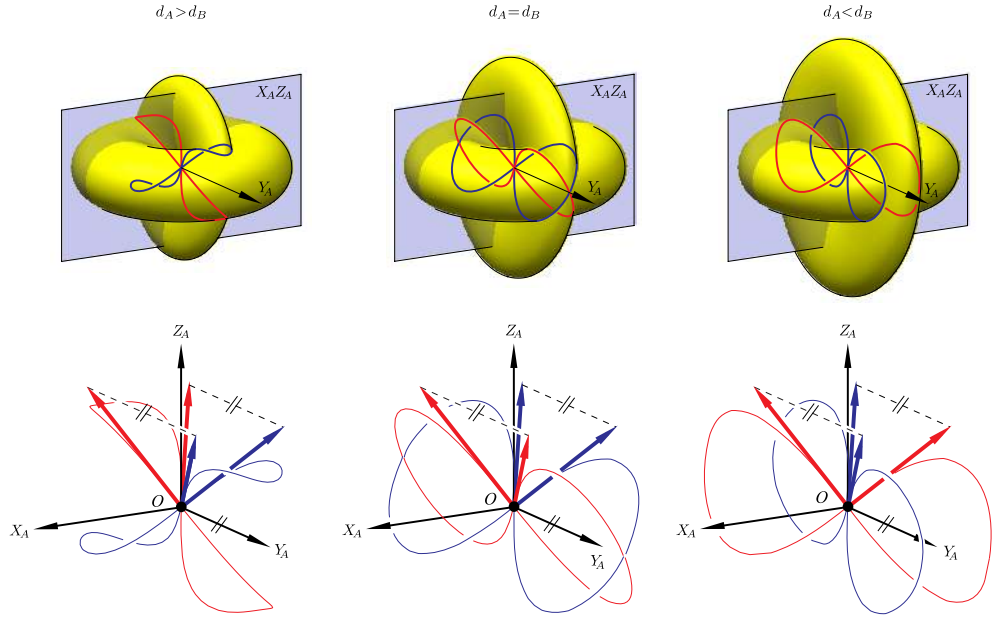

Fig. 11. Tangent vectors to the intersection curves at the double singularity, for the three possible cases: $r_A > r_B$, $r_A = r_B$ and $r_A < r_B$

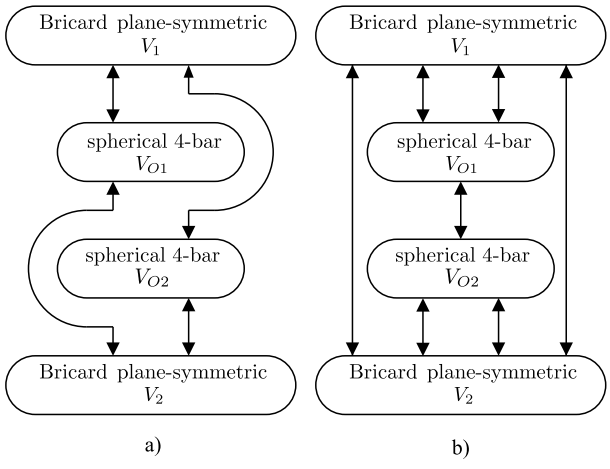

Fig. 12. Two cases of branch reconfiguration diagrams when the intersection of concentric singular toroids is composed of two singular curves: a) $r_A < r_B$ and $\gamma_A \neq \gamma_B$ (example presented in this subsection); b) $r_A = r_B$ and $|\gamma_A| = |\gamma_B|$.

.

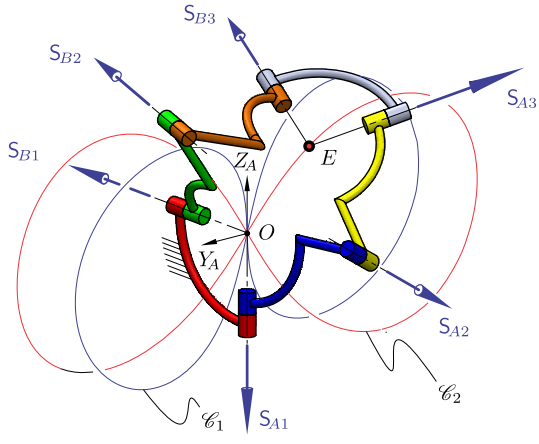

Fig. 13. A reconfigurable Bricard plane-symmetric linkage that allows the reconfiguration between two spherical 4R branches through two Bricard branches. The intersection of the concentric singular toroids is composed of two singular curves.

.

Conclusions

The plane-symmetric case of Bricard loops was analyzed using the intersection of two concentric singular toroids, allowing the design of reconfigurable linkages with several motion branches which can be either plane-symmetric 6R branches or spherical 4R branches. The conditions for having two singular curves in the intersection set were presented. Each of these curves is related to a plane-symmetric 6R branch of motion. The phenomenon of double singularity leads to kinematotropy when the two surface generators are joined by a spherical pair or a reduction of this to a pair of revolute joints each being parallel to the axis of rotation of surfaces of revolution. However, in the case of overconstrained plane-symmetric linkages it was found that such double singularity leads to a spherical 4R branch.

The study of the escape directions, which are the tangents to the intersection curves at the double singularity revealed the existence of linkages whose evolved crank-rocker spherical 4R linkage can work in its two branches without disassembling it. To the knowledge of the authors, this is the first time that a linkage with this property is presented. These interesting results, along with those for the line-symmetric case, which the authors are presenting in a different paper, shed light on whether it is possible to design more overconstrained linkages that can be reconfigured between different branches using the method of generated surfaces. The paper in which the authors apply the method to the line-symmetric case, [44], is published in parallel with this paper.

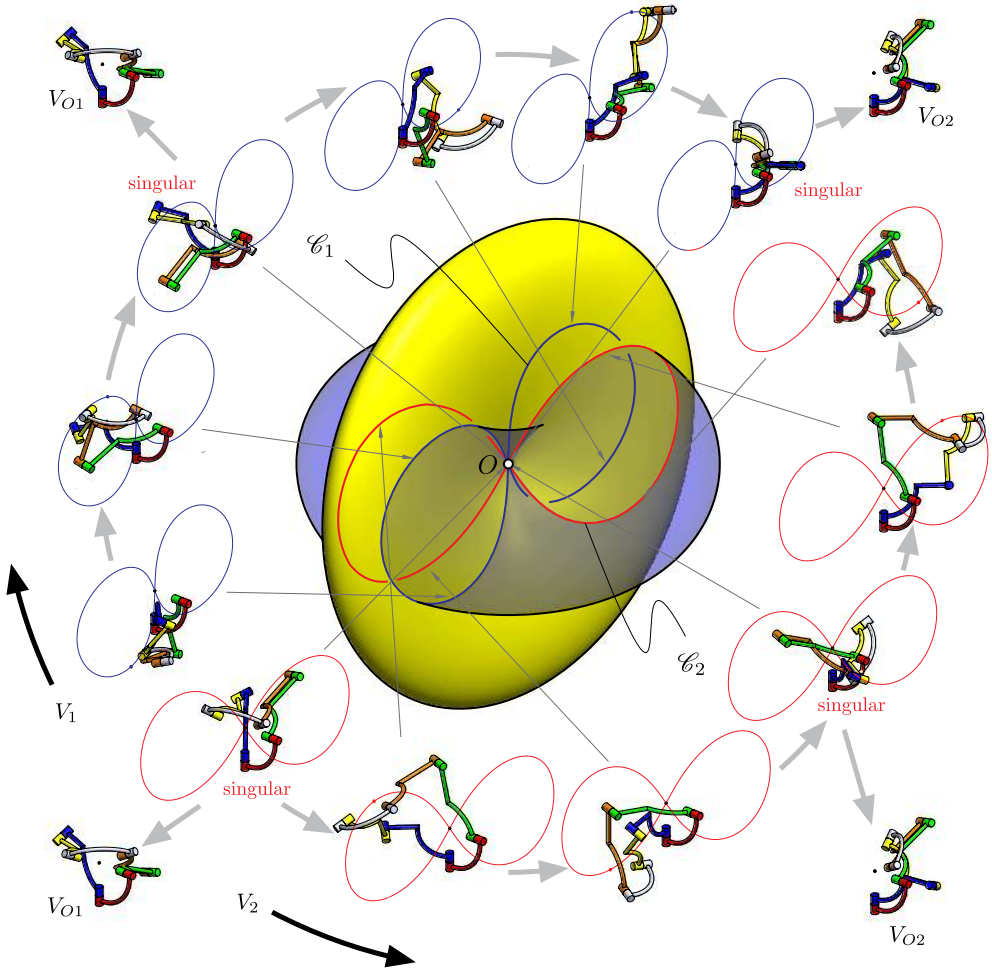

Fig. 14. Several configurations of the plane-symmetric Bricard linkage when the intersection of concentric toroids contains two singular curves.

.

Acknowledgements

The authors gratefully acknowledge the support from the EU 7th Framework Programme, Clearing Clutter Bit by Bit (SQUIRREL), under grant No.610532 and the EPSRC project EP/P026087/1. The first author would like to thank the The Mexican National Council for Science and Technology (CONACyT) for the scholarship awarded to pursue doctoral studies as well as the Mexican Ministry of Public Education (SEP) for the complementary funding awarded for the same aim.

References

[1] Bricard, R., 1897. "Mémoire sur la thèorie de l'octaèdre articulè". *Journal of Pure and Applied Mathematics,* **3**, pp. 113–150.

[2] Bricard, R., 1927. *Leçons de cinématique*. Gauthier-Villars, Paris, France.

[3] Hunt, K. H., 1967. "Screw axes and mobility in spatial mechanisms via the linear complex". *Journal of Mechanisms,* **2**(3), pp. 307–327.

[4] Phillips, J., 1990. *Freedom in Machinery: Volume 2, Screw Theory Exemplified*. Cambridge University Press, Cambridge ,UK.

[5] Baker, J. E., 1980. "An analysis of the Bricard linkages". *Mechanisms and Machine Theory,* **15**, pp. 267–286.

[6] Dai, J. S., and Gogu, G., 2016. "Special issue on reconfigurable mechanisms: Morphing, metamorphosis and reconfiguration through constraint variations and reconfigurable joints". *Mechanism and Machine Theory,* **96, Part 2**, pp. 213 – 214. Reconfigurable mechanisms.

[7] Kuo, C. H., Dai, J. S., and Yan, H. S., 2009. "Reconfiguration principles and strategies for reconfigurable mechanisms". In Reconfigurable Mechanisms and Robots, 2009. ReMAR 2009. ASME/IFToMM International Conference on, pp. 1–7.

[8] Wohlhart, K., 1996. "Kinematotropic linkages". In Recent Advances in Robot Kinematics, J. Lenarčič and V. Parent-Castelli, eds., Portoroz, Slovenia. Dordrecht: The Netherlands, pp. 359–368.

[9] Galletti, C., and Fanghella, P., 2001. "Single-loop kinematotropic mechanisms". *Mechanism and Machine*

Theory, **36**(3), pp. 743–761.

[10] Dai, J. S., and Jones, J. R., 1999. "Mobility in metamorphic mechanisms of foldable/erectable kinds". *Transactions of the ASME: Journal of Mechanical Design,* **121**(3), pp. 375–382.

[11] Zhang, K., Dai, J. S., and Fang, Y., 2013. "Geometric constraint and mobility variation of two 3SvPSv metamorphic parallel mechanisms". *ASME Journal of Mechanical Design,* **135**(1), pp. 011001–011001–8.

[12] Gan, D., Dai, J. S., Dias, J., and Lakmal, S., 2013. "Unified kinematics and singularity analysis of a metamorphic parallel mechanism with bifurcated motion". *Journal of Mechanisms and Robotics,* **135**(1), pp. 031004–031004–11.

[13] S., L., and Dai, J. S., 2012. "Structure synthesis of single-driven metamorphic mechanisms based on the augmented Assur groups". *Journal of Mechanisms and Robotics,* **4**(3), pp. 031004–031004–8.

[14] Qin, Y., Dai, J., and Gogu, G., 2014. "Multi-furcation in a derivative queer-square mechanism". *Mechanism and machine theory,* **81**, 11, pp. 36–53.

[15] Ye, W., Fang, Y., Zhang, K., and Guo, S., 2014. "A new family of reconfigurable parallel mechanisms with diamond kinematotropic chain". *Mechanism and Machine Theory,* **74**, pp. 1 – 9.

[16] Kong, X., 2014. "Reconfiguration analysis of a 3-DOF parallel mechanism using Euler parameter quaternions and algebraic geometry method". *Mechanism and Machine Theory,* **74**, pp. 188–201.

[17] Kong, X., 2012. "Type synthesis of variable degrees-of-freedom parallel manipulators with both planar and 3T1R operation modes". In Proceedings of the ASME 2012 International Design Engineering Technical Conferences, Chicago, IL, U.S.A., pp. 497–504. Paper number DETC2012-70621.

[18] Zhang, K., and Dai, J. S., 2016. "Geometric constraints and motion branch variations for reconfiguration of single-loop linkages with mobility one". *Mechanism and Machine Theory,* **106**, pp. 16 – 29.

[19] López-Custodio, P. C., Rico, J. M., and Cervantes-Sánchez, J. J., 2017. "Local analysis of helicoid-helicoid intersections in reconfigurable linkages". *ASME Journal of Mechanisms and Robotics,* **9**(3), pp. 031008 – 031008–17.

[20] Arponen, T., Müller, A., Piipponen, S., and Tuomela, J., 2014. "Kinematical analysis of overconstrained and underconstrained mechanisms by means of computational algebraic geometry". *Meccanica,* **49**(4), Apr, pp. 843–862.

[21] Zhang, K., Müller, A., and Dai, J. S., 2016. "A novel reconfigurable 7r linkage with multifurcation". In Advances in Reconfigurable Mechanisms and Robots II, X. Ding, X. Kong, and J. S. Dai, eds., Springer International Publishing, pp. 3–14.

[22] Aimedee, F., Gogu, G., Dai, J., Bouzgarrou, C., and Bouton, N., 2016. "Systematization of morphing in reconfigurable mechanisms". *Mechanism and machine theory,* **96**(Part 2), 2, p. 215224.

[23] López-Custodio, P. C., Rico, J. M., Cervantes-Sánchez, J. J., Pérez-Soto, G. I., and Díez-Martínez, C. R., 2017. "Verification of the higher order kinematic analyses equations". *European Journal of Mechanics - A/Solids,* **61**, pp. 198 – 215.

[24] Müller, A., 2016. "Local kinematic analysis of closed-loop linkages mobility, singularities, and shakiness". *ASME Journal of Mechanisms and Robotics,* **8**(4), pp. 041013–1—041013–11.

[25] Müller, A., 2005. "Geometric characterization of the configuration space of rigid body mechanisms in regular and singular points". In International Design Engineering Technical Conferences and Computers and Information in Engineering Conference, pp. 827–840.

[26] Kong, X., 2016. "Kinematic analysis of conventional and multi-mode spatial mechanisms using dual quaternions". In Proceedings of the ASME 2016 International Design Engineering Technical Conferences, Vol. 5B, Charlotte, North Carolina, USA, pp. V05BT07A085–1—V05BT07A085–10. Paper number DETC2016-59194.

[27] Song, C. Y., Chen, Y., and Chen, I.-M., 2013. "A 6R linkage reconfigurable between the line-symmetric Bricard linkage and the Bennett linkage". *Mechanism and Machine Theory,* **70**, pp. 278 – 292.

[28] Chen, Y., and Chai, W. H., 2011. "Bifurcation of a special line and plane symmetric Bricard linkage". *Mechanism and Machine Theory,* **46**(4), pp. 515 – 533.

[29] Zhang, K., and Dai, J., 2014. "A kirigami-inspired 8R linkage and its evolved overconstrained 6R linkages with the rotational symmetry of order two". *ASME Journal of Mechanisms and Robotics,* **6**(2), pp. 021007–021007–12.

[30] Jenkins, E. M., Crossley, F. R. E., and Hunt, K. H., 1969. "Gross motion attributes of certain spatial mechanisms". *Journal of Engineering for Industry,* **91**(1), pp. 83–90.

[31] Torfason, L. E., and Crossley, F. R. E., 1971. "Use of the intersection of surfaces as a method for design of spatial mechanisms". In Proceedings of the 3rd World Congress for the Theory of Machines and Mechanisms, Vol. **B**, Kupari, Yugoslavia, pp. 247–258. Paper B-20.

[32] Hunt, K. H., 1973. "Constant-velocity shaft couplings: a general theory". *Journal of Engineering for Industry,* **95**(2), pp. 455–464.

[33] Fichter, E. F., and Hunt, K. H., 1975. "The fecund torus, its bitangent-circles and derived linkages". *Mechanism and Machine Theory,* **10**(2-3), pp. 167–176.

[34] Shrivastava, A. K., and Hunt, K. H., 1973. "Dwell motion from spatial linkages". *Transactions of the ASME: Journal of Engineering for Industry,* **95**(2), pp. 511–518.

[35] Torfason, L. E., and Sharma, A. K., 1973. "Analysis of spatial RRGRR mechanisms by the method of generated surfaces". *Transactions of the ASME: Journal of Engineering for Industry,* **95**(3), pp. 704–708.

[36] Su, H. J., and McCarthy, J. M., 2005. "Dimensioning

a constrained parallel robot to reach a set of task positions". In Proceeding of the 2005 IEEE International Conference on Robotics and Automation, Barcelona, Spain, pp. 4026–4030.

[37] Liu, Y., and Zsombor-Murray, P., 1995. "Intersection curves between quadric surfaces of revolution". *Transactions of the Canadian Society for Mechanical Engineering,* **19**(4), pp. 435–453.

[38] López-Custodio, P. C., Rico, J. M., Cervantes-Sánchez, J. J., and Pérez-Soto, G., 2016. "Reconfigurable mechanisms from the intersection of surfaces". *ASME Journal of Mechanisms and Robotics,* **8**(2), pp. 021029–1-—021029–19.

[39] Lee, C. C., and Hervé, J. M., 2012. "A discontinuously movable constant velocity shaft coupling of Koenigs joint type". In Advances in Reconfigurable Mechanisms and Robots I, M. Z. Jx Sx Dai and X. Kong, eds., pp. 35–43.

[40] Phillips, J., 1984. *Freedom in Machinery: Volume 1, Introducing Screw Theory*. Cambridge University Press, Cambridge ,UK.

[41] Hunt, K. H., 1978. *Kinematic Geometry of Mechanisms*. Oxford University Press, New York, USA.

[42] Hunt, K. H., 1968. "Note on complexes and mobility". *Journal of Mechanisms,* **3**(3), pp. 199 – 202.

[43] Chen, Y., and You, Z., 2009. "Two-fold symmetrical 6r foldable frame and its bifurcations". *International Journal of Solids and Structures,* **46**(25), pp. 4504 – 4514.

[44] López-Custodio, P. C., Dai, J. S., and Rico, J. M., 2017. "Branch reconfiguration of Bricard loops based on toroids intersections: Line-symmetric case". *Manuscript submitted for publication*.

[45] Liu, X.-M., Liu, C.-Y., Yong, J.-H., and Paul, J.-C., 2011. "Torus/torus intersection". *Computer-Aided Design and Applications,* **8**(3), pp. 465–477.

[46] Krivoshapko, S. N., and Ivanov, V. N., 2015. *Encyclopedia of Analytical Surfaces*. Springer, Switzerland.

[47] Thorpe, J. A., 1979. *Elementary Topics in Differential Geometry*. Springer-Verlag, New York, USA.

[48] Whitney, H., 1965. "Tangents to an analytic variety". *Annals of Mathematics,* **81**, pp. 496 – 549.

[49] Lerbet, J., 1998. "Analytic geometry and singularities of mechanisms". *Zeitschrift für Angewandte Mathematik und Mechanik.,* **78**(10), pp. 687–694.

[50] Müller, A., 2002. "Local analysis of singular configuration of open and closed loop manipulators". *Multibody System Dynamics,* **8**(3), pp. 297–326.

[51] Müller, A., 2014. "Higher derivatives of the kinematic mapping and some applications". *Mechanism and Machine Theory,* **76**, pp. 70 – 85.

[52] Diez-Martínez, C. R., Rico, J. M., and Cervantes-Sánchez, J. J., 2006. "Mobility and connectivity in multiloop linkages". In Advances in Robot Kinematics, J. Lenarčič and B. Roth, eds., Springer Netherlands, pp. 455–464.

[53] Connelly, R., and Servatius, H., 1994. "Higher-order rigidity—what is the proper definition?". *Discrete & Computational Geometry,* **11**(2), Feb, pp. 193–200.

[54] Gupta, K. C., and Ma, R., 1995. "A direct rotatability criterion for spherical four-bar linkages". *Journal of Mechanical Design,* **117**(4), p. 597600.

[55] Waldron, K. J., 1976. "Elimination of the branch problem in graphical Burmester mechanism synthesis for four finitely separated positions". *Journal of Engineering for Industry,* **98**(1), pp. 176–182.

[56] Reinholtz, C. F., Sandor, G. N., and Duffy, J., 1986. "Branching analysis of spherical RRRR and spatial RCCC mechanisms". *Journal of Mechanisms, Transmissions, and Automation in Design,* **108**(4), p. 481486.

List of Figures